Analyses of the Recycling Receptor, FcRn, in Live Cells Reveal Novel Pathways for Lysosomal Delivery

Zhuo Gan[1,2], Sripad Ram[2], Carlos Vaccaro[2], Raimund J. Ober[2,3,*] and E. Sally Ward[2,*]

[1]*Biomedical Engineering Graduate Program, University of Texas Southwestern Medical Center at Dallas, Dallas, TX 75390, USA*
[2]*Department of Immunology, University of Texas Southwestern Medical Center at Dallas, Dallas, TX 75390, USA*
[3]*Department of Electrical Engineering, University of Texas at Dallas, Richardson, TX 75080, USA*
Corresponding authors: E. Sally Ward, sally.ward@utsouthwestern.edu and Raimund J. Ober, ober@utdallas.edu

Lysosomes play a central role in the degradation of proteins and other macromolecules. The mechanisms by which receptors are transferred to lysosomes for constitutive degradation are poorly understood. We have analyzed the processes that lead to the lysosomal delivery of the Fc receptor, FcRn. These studies provide support for a novel pathway for receptor delivery. Specifically, unlike other receptors that enter intraluminal vesicles in late endosomes, FcRn is transferred from the limiting membrane of such endosomes to lysosomes, and is rapidly internalized into the lysosomal lumen. By contrast, LAMP-1 persists on the limiting membrane. Receptor transfer is mediated by tubular extensions from late endosomes to lysosomes, or by interactions of the two participating organelles in kiss-and-linger-like processes, whereas full fusion is rarely observed. The persistence of FcRn on the late endosomal limiting membrane, together with selective transfer to lysosomes, allows this receptor to undergo recycling or degradation. Consequently, late endosomes have functional plasticity, consistent with the presence of the Rab5 GTPase in discrete domains on these compartments.

Key words: Endosomal trafficking, FcRn, LAMP-1, lysosome, Rab GTPase

Protein biosynthesis and breakdown represent fundamental aspects of cellular homeostasis. Lysosomes constitute the primary intracellular site for the degradation of proteins and other macromolecules on the endocytic pathway (1,2). How proteins or other lysosomally directed macromolecules such as membrane receptors or cargo transit from endosomes to lysosomes is an area of active discussion. Multiple models, including those involving vesicular transport, endosomal maturation or late endosomal-lysosomal fusion have been proposed for the delivery of such macromolecules to these degradative compartments (2–6). Recent studies using labeled dextran as a fluid-phase tracer have provided direct support for late endosomal-lysosomal fusion involving different processes, ranging from transient kiss-and-run processes or more prolonged kiss-and-linger interactions to complete fusion to generate a hybrid organelle (5). By contrast, there is limited knowledge concerning how membrane receptors migrate from late endosomes into these degradative compartments.

Despite the lack of knowledge concerning how late endosomes deliver their membrane receptors to lysosomes, it is known that the entry of receptors into intraluminal vesicles (ILVs) of late endosomes (or multivesicular bodies, MVBs) prior to lysosomal delivery can occur via ubiquitin-dependent and -independent pathways (7–11). In addition, the molecular mechanisms involved in the sorting of ubiquitinated receptors from the limiting membrane of late endosomes into ILVs of MVBs have been intensively studied (7–9,11,12), whereas ubiquitin-independent pathways are less well characterized (9–11). Although inhibition of entry of ubiquitin-dependent receptors such as the EGF receptor into ILVs reduces its degradative rate (13), the fundamental question persists as to whether ILV entry into MVBs is a prerequisite for the lysosomal degradation of membrane proteins.

The central role of Rab GTPases in orchestrating intracellular trafficking is becoming increasingly apparent and has direct relevance to lysosomal biogenesis (14–16). These GTPases accumulate on the surface of vesicular or tubular compartments such as endosomes where they recruit effectors that can induce membrane tethering prior to homo- or heterotypic fusion. The Rab proteins, Rab5 and Rab7, are associated with early/sorting and late endosomal trafficking, respectively (17–20). For example, Rab7 is involved in regulating both late endosomal mobility and MVB formation (21). Recent studies have demonstrated that early (sorting) endosomes can mature into late endosomes by a process known as 'Rab conversion' in which Rab5 is gradually replaced by Rab7 (22). On the basis of these observations, a model has been proposed in which all Rab5 is dissociated from maturing Rab7^{+} endosomes prior to their fusion with lysosomes (22). However, there is limited knowledge concerning the point at which the contents of an endosome can no longer be recycled and become irreversibly destined for degradation. This is particularly relevant for the constitutive degradation of receptors such as the transferrin receptor and the Fc

receptor, FcRn, for which the primary routing is recycling back to the plasma membrane (23–26).

In the current study, we have analyzed the processes that lead to the constitutive, intracellular degradation of the Fc receptor, FcRn (24,27). This Fc receptor follows both recycling and transcytotic pathways to transport its immunoglobulin G (IgG) ligand within and across cells of diverse origin (23,28–31). FcRn plays a central role in regulating IgG concentrations and transport *in vivo* (24), and defects in this receptor result in hypogammaglobumenia (32–34). The constitutive degradation of FcRn, therefore, not only has broad relevance to understanding how (recycling/transcytotic) receptor levels are maintained, but also impacts a fundamental aspect of humoral immunity.

Our live-cell-imaging analyses of FcRn in endothelial cells provide support for novel pathways for lysosomal delivery. This Fc receptor remains associated with the limiting membrane of the late endosome until endosomal-lysosomal contact occurs, whereupon transferred FcRn rapidly accumulates in the lysosomal vacuole. The majority of transfer events from late endosomes to lysosomes do not involve full fusion, but instead are mediated by either tubular connections or close interactions between participating organelles in processes that resemble kiss-and-linger (5,6,35,36). The persistence of FcRn on the limiting membrane of late endosomes, rather than accumulation in ILVs, combined with selective transfer events to lysosomes allows this receptor to be either recycled or degraded. These processes confer functional plasticity on endosomes until an unexpectedly late stage in their maturation. Consistent with retention of plasticity, (late) endosomes that are associated with both Rab5 and Rab7 can interact with lysosomes. Our data, therefore, indicate that Rab7 acquisition without complete loss of Rab5 demarcates late endosomes that are competent to transfer material to lysosomes.

Results

Distribution of FcRn
HMEC-1 cells were transfected with mRFP-tagged FcRn (human) and pulse-chased with Alexa 647-labeled dextran to label lysosomes (2 hours pulse, 6–24 hours chase). mRFP fluorescence could be clearly detected in the intraluminal space of the dextran+ lysosomes, in addition to being present on the limiting membrane of abundant early endosomes as described previously (23) (Figure 1A). FcRn is a type I membrane protein, so that C-terminal tagging results in the localization of the fluorescent protein in the cytosol if the receptor is on the limiting membrane of intracellular organelles. Importantly, the detection of mRFP in the intraluminal space is not due to cleavage of mRFP from FcRn on the limiting lysosomal membrane followed by release into the lumen, since it is observed for both N- and C-terminally tagged FcRn. In cells transfected with C-terminally tagged FcRn,

94% (n = 50) of dextran+ lysosomes are mRFP+ and for N-terminally tagged FcRn, 96% (n = 55) of dextran+ lysosomes are mRFP+, indicating that the fusion of mRFP to FcRn does not impact the intracellular trafficking pathway of FcRn. However, from the analyses using mRFP-tagged FcRn, we could not determine whether FcRn is also present on the limiting membranes of lysosomes in addition to the intraluminal spaces. We therefore also carried out experiments with FcRn tagged at the C-terminus with GFP (FcRn-GFP) to investigate this. GFP has very low fluorescence at lysosomal pH (37,38) and is susceptible to proteolysis (38–40). We hypothesized that GFP fluorescence from C-terminally tagged FcRn would not be detectable if FcRn were rapidly internalized into the intraluminal space following transfer to lysosomes. Although GFP-labeled FcRn could be seen on the limiting membrane of endosomes as described previously (23), we did not observe GFP in lysosomes when the fluorophore was linked to either the N- or C-terminus of FcRn (Figure 1, and data not shown). This suggests that the internalization of FcRn from the limiting membrane into the intraluminal space of lysosomes is relatively rapid, so that the steady state distribution is primarily within the lumen. The lysosomal accumulation of FcRn is most likely due to the constitutive turnover of this receptor.

Temporal aspects of lysosomal delivery
The constitutive expression of mRFP-tagged FcRn in transfected cells precludes an analysis of the temporal aspects of lysosomal delivery of this receptor. We therefore used a fluorescently labeled IgG ('MST-HN') that has been engineered to bind through its Fc region with high affinity to FcRn in the pH range 5–7.4 ((41), data not shown) to track receptor behavior over time periods that could be regulated by IgG delivery. In addition, to facilitate the use of labeled IgG as a tag for FcRn, a mutated variant of human FcRn (42) that is engineered to have higher affinity for IgG was used throughout these studies. The relatively high affinity of the interaction of this mutated FcRn for binding to MST-HN in the range pH 6.0–7.2 (K_D at pH 6.0 = 1 nM; K_D at pH 7.2 = 4.5 nM, (43)) reduces the possibility of dissociation of MST-HN from FcRn in endosomes and at the cell surface so that it can be used as a tracer for FcRn on both the recycling and endolysosomal pathways within cells. By contrast, wild-type IgG1 binds with substantially lower affinity to FcRn (mutant) at pH 6.0 and with immeasurably low affinity at near-neutral pH (41,42) and is therefore unsuitable as a ligand for tracking FcRn.

mRFP-FcRn-transfected cells were pulse-chased with Alexa 488-labeled dextran (MW 10 000 Da) to label lysosomes, followed by addition of 5 μg/ml Atto 647N-labeled IgG. Cells were imaged at different times up until 24 hours following IgG addition (Figure 1B). After a pulse time of ∼1-3 hours with labeled IgG, the antibody shows extensive colocalization with mRFP-FcRn (Figure 1B; or FcRn-mRFP, data not shown) in endosomal structures or

smaller tubulovesicular compartments (all of 50 mRFP-FcRn$^+$ or FcRn-mRFP$^+$ endosomes analyzed are IgG$^+$), consistent with our earlier studies (41) with little or no colocalization with lysosomes (2% of 51 dextran$^+$ FcRn$^+$ lysosomes analyzed are IgG$^+$). However, following 4–6 hours of IgG addition, significant amounts of labeled antibody are colocalized with dextran and mRFP in the intraluminal space of lysosomes (Figure 1B; 85% of 46 dextran$^+$ FcRn$^+$ lysosomes analyzed are IgG$^+$), although a substantial proportion of this antibody remains associated with FcRn in endosomes (Figure 1B; all of 62 FcRn$^+$ endosomes analyzed are IgG$^+$). At longer times (6–24 hours), the amount of IgG in lysosomes relative to endosomes increases, until about 16–24 hours when the majority is located in lysosomes (Figure 1B; 98% of 50 dextran$^+$ FcRn$^+$ lysosomes analyzed are IgG$^+$). Thus, within several hours of addition, IgG ligand and FcRn can be detected in the intraluminal space of lysosomes, and the accumulation continues to increase thereafter. The behavior of the MST-HN mutant contrasts with that of wild-type IgGs which, on account of their marked pH-dependent binding to FcRn, are in general sorted into the recycling/transcytotic pathway and exocytosed

(23,44). Since the MST-HN mutant is an effective tag of FcRn, this data establishes the timing of FcRn transfer to lysosomes.

Modes of FcRn transport from late endosomes to lysosomes

To analyze the details of the dynamic processes that are involved in the transfer of FcRn to lysosomes, HMEC-1 cells were cotransfected with mRFP-FcRn and lysosomal-associated membrane protein-1 (LAMP-1)-GFP to demarcate late endosomes (dim for LAMP-1, mannose-6-phosphate receptor (M6PR) positive and dextran negative; data not shown) and lysosomes (bright for LAMP-1, M6PR negative, dextran positive). The use of fluorescently labeled LAMP-1 allows the limiting membrane of the lysosomes to be demarcated. Consistent with the analyses using dextran-pulsed cells (Figure 1), mRFP could be detected in the intraluminal space of LAMP−1$^+$ (bright) lysosomes (Figure 2).

Figure 2A shows the delivery of mRFP-labeled FcRn from a late endosome to a closely apposed lysosome via a tubule that extends from the late endosome (13.5 s),
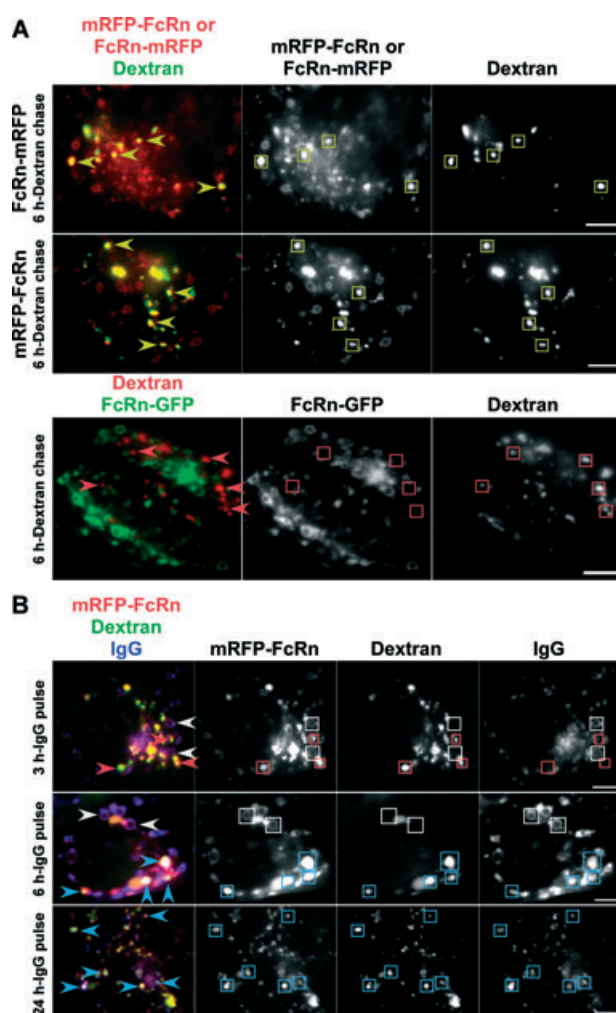

Figure 1: mRFP-tagged FcRn can be detected in the lysosomes of transfected HMEC-1 cells. HMEC-1 cells were cotransfected with mRFP-FcRn (human) and human β_2m, FcRn-mRFP (human) and human β_2m, or FcRn-GFP (human) and human β_2m, as indicated. Cells were pulsed with Alexa 647- (A) or 488- (B) labeled dextran for 2 hours and chased for 1 (B) or 6 hours (A). Compartments in the single color data for FcRn, dextran and IgG are highlighted with rectangles of the same colors as the arrowheads. Scale bars = 5 μm. A, yellow arrowheads in the upper panels indicate dextran$^+$ lysosomes with mRFP-tagged FcRn in the intraluminal space. Both N- or C-terminally tagged FcRn can be detected in lysosomes. Red arrowheads in the lower panels indicate dextran$^+$ lysosomes without detectable FcRn-GFP in the intraluminal space. B, after dextran pulse-chase, cells were incubated with Atto 647N-labeled IgG for different times as indicated. White arrowheads indicate endosomes with mRFP-FcRn$^+$ IgG$^+$ limiting membranes. Red arrowheads indicate mRFP-FcRn$^+$ dextran$^+$ lysosomes without detectable IgG following 3 hours of IgG incubation. Blue arrowheads indicate mRFP-FcRn$^+$ dextran$^+$ IgG$^+$ lysosomes following 6 or 24 hours of IgG incubation.
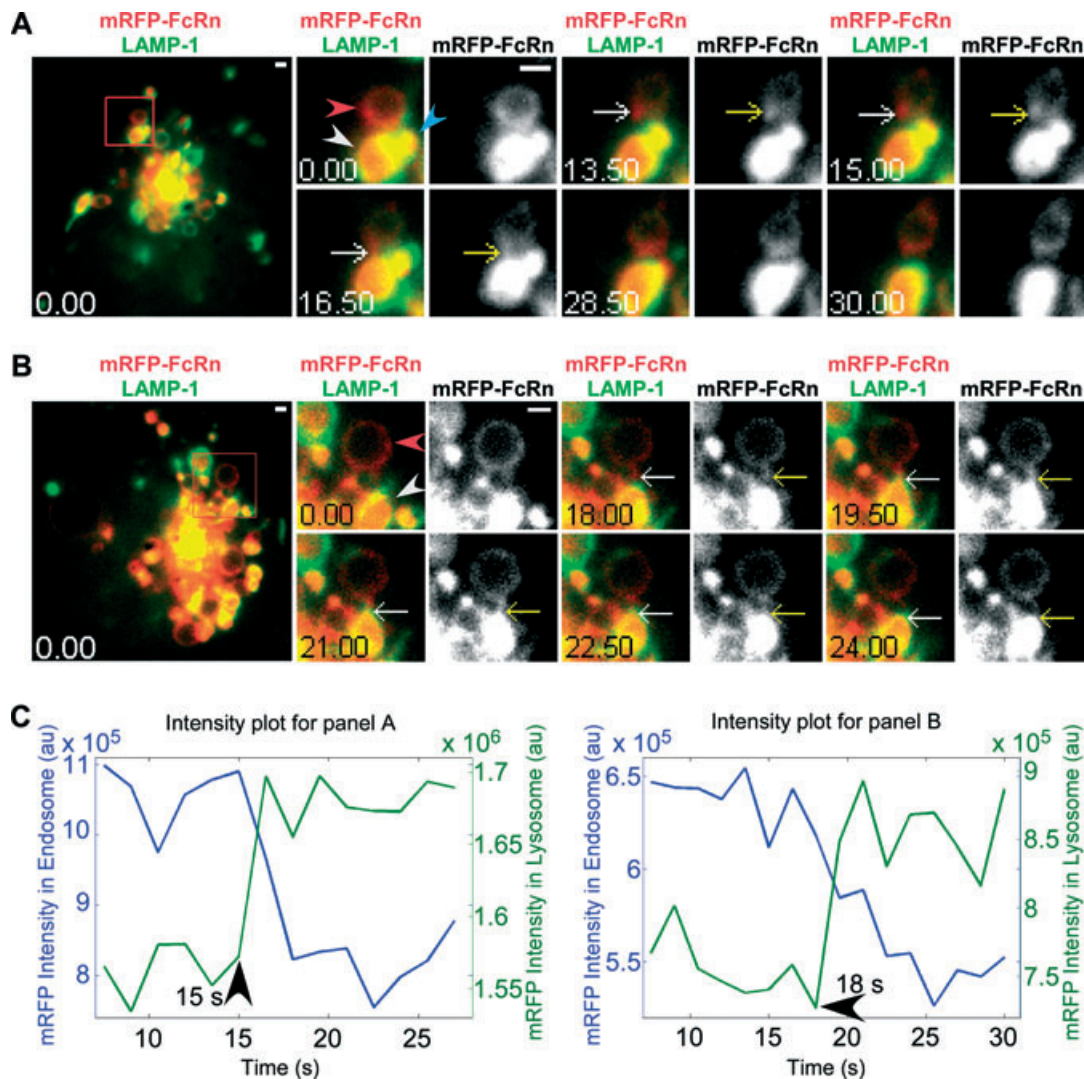
Figure 2: Tubule-mediated transfer of FcRn from the limiting membrane of late endosomes to the intraluminal space of lysosomes. HMEC-1 cells were cotransfected with LAMP-1-GFP, mRFP-FcRn (human) and human β_2m. Individual images in A and B are presented with the time (in seconds) at which each image was acquired (first image is arbitrarily set to time 0). Images on the left hand side show complete cells, with the boxed regions expanded as cropped images for the 0 second and later images. White arrows in the overlay images show the events of interest that are also indicated in the single color (mRFP-FcRn) data by yellow arrows. Images shown in A and B are individual frames of Movies S1 and S2, respectively. Scale bars = 1 μm. A, a mRFP-FcRn+ tubule extends from a late endosome (red arrowhead) to a lysosome (white arrowhead) from 13.5–16.5 s. At 16.5 s, the tubule merges with the lysosome and separates from the late endosome. An additional lysosome (blue arrowhead, 0 s) merges with the first lysosome (white arrowhead at 0 s) at 28.5–30 s. B, a mRFP-FcRn+ tubule extends from a late endosome (red arrowhead) towards a lysosome (white arrowhead) at 0 s, merges with the lysosome at 19.5 s and breaks away from the recipient lysosome at 24 s. C, the fluorescence intensity plots for mRFP in the interacting compartments in A and B, with times of initiation of transfer indicated.

fuses with a lysosome and immediately separates from the 'donor' endosome within a time period of about 3 s. Subsequent to FcRn transfer, a smaller lysosome fuses with the first lysosome in a homotypic fusion event (28.5–30 s). In Figure 2B, a FcRn+ tubule that is longer than that shown in Figure 2A is extended from a late endosome and delivers FcRn to the lysosome. This tubule merges with the lysosome (19.5 s) and disconnects from the lysosome 4.5 s following the merging event. The intensity changes for mRFP fluorescence in both

the donor endosome (decrease in intensity) and the acceptor lysosome (increase in intensity) for these two transfer events are shown in Figure 2C. For all intensity plots in this study, to exclude the possibility that the intensity decreases in donor compartments are due to photobleaching, the average photobleaching rates were determined. The average intensity decays are much less than the measured intensity decreases in donor compartments, indicating that intensity decreases in donor compartments are not due to photobleaching

(Figures S1 and S2 in Supporting Information). In both examples of transfer events, the lysosomes already have substantial amounts of mRFP (FcRn) in their vacuole. Taken together with the absence of FcRn-GFP on the limiting membrane of lysosomes (Figure 1A), this suggests that the internalization of FcRn into the intraluminal space is efficient.

Due to the constitutive expression of mRFP in transfected cells, the 'brightness' of mRFP in the majority of recipient lysosomes limited our ability to detect relatively small changes in intensity due to transfer of FcRn (tagged with mRFP) to lysosomes. Therefore, to facilitate the analysis of such intensity changes, we further investigated the pathways of late endosome to lysosome transfer using labeled (Atto 647N) MST-HN IgG (41) (Figure 3), for which accumulation in lysosomes only started shortly following IgG addition to cultures. In a subset of analyses, we also used mouse FcRn instead of human FcRn since, unlike human FcRn, it does not have a cytosolic tail lysine (45,46) which could serve as a ubiquitination target (Figure 3C, E, G). Similar distribution and transport modes were observed for both mouse and human FcRn in HMEC-1 cells in this and other studies, indicating that the trafficking pathway of human FcRn from late endosomes to lysosomes is not ubiquitin-dependent (Figure 3, and data not shown).

In Figure 3A, a $FcRn^+$ IgG^+ late endosome interacts via a tubule with a $dextran^+$ IgG^+ lysosome over a time period of 67.5 s (until the data collection is stopped). During a three-second period (43.5–46.5 s), detectable levels of IgG transfer can be observed. The intensity changes for Atto 647N fluorescence in both the donor endosome (decrease in intensity) and the acceptor lysosome (increase in intensity) for this transfer event are presented in Figure 3B. By contrast with Figure 3A, Figure 3C shows IgG transfer between an adjacent late endosome and lysosome via a process that does not involve a detectable tubule and resembles kiss-and-linger events (5,6,35,36). In the example shown, detectable levels of IgG transfer occur over a time period of ~460 s (Figure 3C). An analysis of the intensity changes for Atto 647N fluorescence in the two compartments involved in this transfer event is presented in Figure 3D. The intensity changes over time provide support for the transfer of material from the late endosome to lysosome. In another example of IgG transfer to lysosomes, we observed two tubules extending simultaneously from an $FcRn^+$ IgG^+ endosome (Figure 3E): one tubule interacts with a lysosome for 25.5 s and transfers detectable levels of IgG over a shorter period of 3 s (30–33 s). A second tubule appears to contact an endosome for about 46.5 s. FcRn(-GFP) and IgG could be detected in both tubules (Figure 3E), and instead of separating from the donor endosome, both tubules retract following interaction with their partner organelles. The intensity changes for Atto 647N fluorescence in the donor and acceptor compartments in Figure 3E are consistent with the

transfer of IgG (Figure 3F). Subsequently, FcRn and IgG leave the donor endosome in a tubulovesicular transport container (Figure 3G), suggesting that late endosomes can both transfer FcRn and/or ligand to lysosomes and generate recycling compartments.

Collectively, our analyses indicate that the majority (71%, n = 24 from 24 different cells) of transfer events for FcRn involve tubular extensions from late endosomes to lysosomes, with the remainder resembling kiss-and-linger (5 events) or rarely, full fusion to form hybrid compartments (2 events; data not shown). However, the frequency of kiss-and-linger might be an underestimate, since we frequently observed late endosomes and lysosomes in close proximity without detectable transfer of material. Of the 17 events for which tubular transfer could be observed, 88% involved long-lived contacts between late endosomes and lysosomes (>3 s). All 5 transfer events that did not occur via visible tubules involved contact between participating organelles that lasted for prolonged time periods (>200 s).

Bifurcation of LAMP-1 and FcRn trafficking pathways at the late endosomal-lysosomal transition

LAMP-1 is colocalized with FcRn on the limiting membrane of late endosomes but, in contrast to FcRn, can also be clearly seen on this membrane of lysosomes (Figure 2). For comparative purposes, we therefore analyzed the behavior of LAMP-1 during late endosomal-lysosomal fusion events. These studies indicated that late endosomes (weakly $LAMP-1^+$, $FcRn^+$ and $M6PR^+$) can interact with lysosomes (strongly $LAMP-1^+$, $M6PR^-$) to transfer LAMP-1 through processes that involve tubular extensions from the late endosomes. In Figure 4A, a tubule can be seen extending from the lower part of the late endosomes at 0 s. This tubule then appears to form a vesicular compartment that moves around the perimeter of the late endosome prior to extending as a tubule at 39 s to fuse with the lysosome to transfer LAMP-1 (40.5–43.5 s). This transfer event is followed by separation of this tubule from the late endosome. The intensity changes for GFP fluorescence in both the donor endosome (decrease in intensity) and the acceptor lysosome (increase in intensity) for this transfer event are presented in Figure 4C. Due to the limited resolution of fluorescence microscopy, it is impossible to conclusively rule out an alternative, less likely interpretation that this moving structure is a separated, small compartment that contacts and moves around the perimeter of the late endosome and subsequently bridges the late endosome and the lysosome.

We also observed that LAMP-1 can migrate from a lysosome to a (late) endosome (Figure 4B). In the example shown, transfers occur in stepwise fashion via two distinct tubules (12–18 and 24–25.5 s). Each of these tubules extends, merges with the limiting membrane of the recipient late endosome and separates from the donor lysosome prior to the delivery of the next
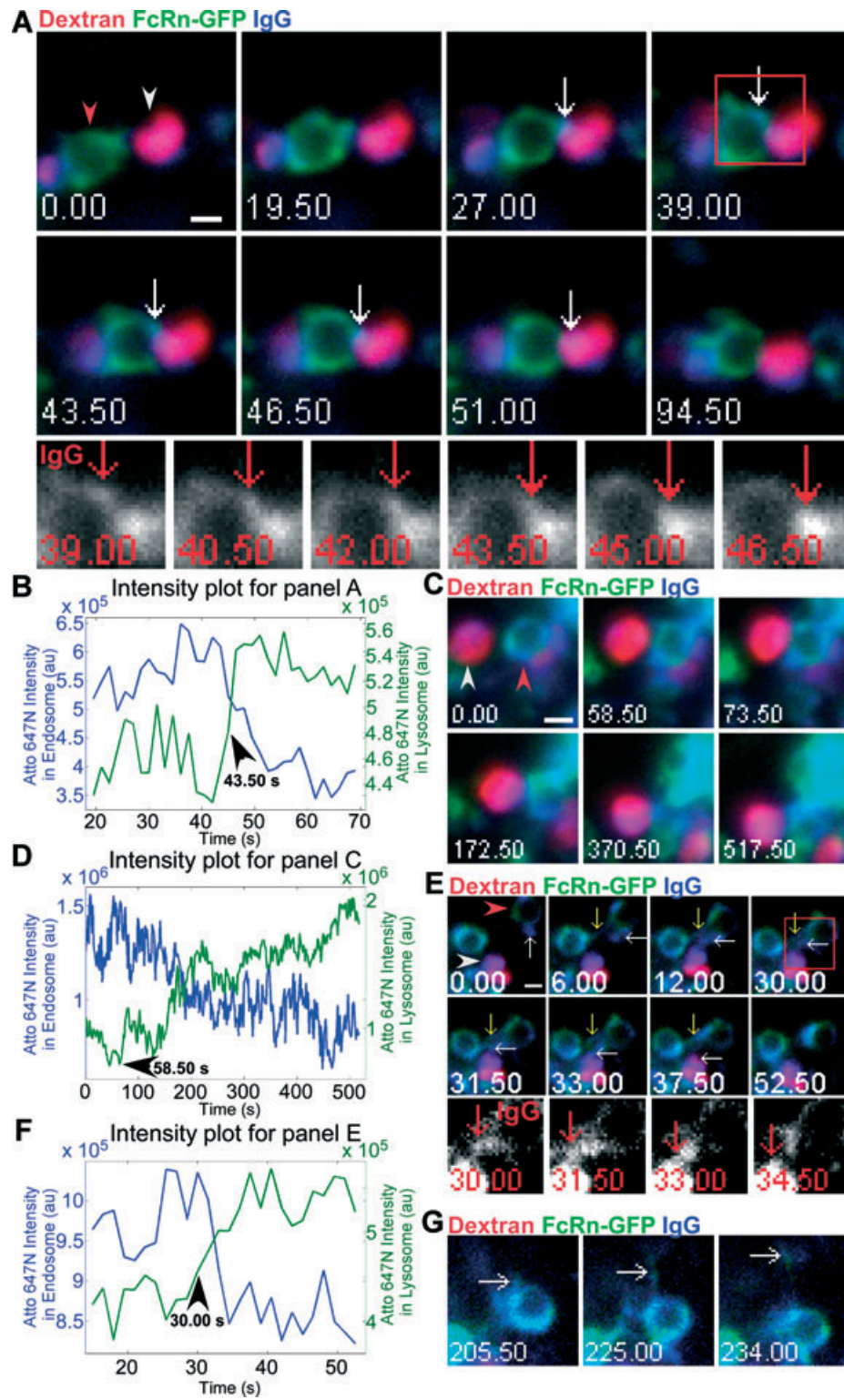
Figure 3: Legend on next page.

tubule. Subsequently, LAMP-1 appears to diffuse into the limiting membrane of the late endosome, although other interpretations are possible such as that this LAMP-1^+ tubulovesicular compartment moves rapidly out of the focal plane. The intensity changes for GFP fluorescence in the donor and acceptor compartments are shown in Figure 4C. This demonstrates that bidirectional movement between the limiting membranes of late endosomes and lysosomes can occur. In all LAMP-1 transfer events (n = 6 from 4 different cells), tubular extensions were observed and we did not detect FcRn nor IgG transfer. Taken together with the distinct distribution of LAMP-1 and FcRn in lysosomes, this indicates that the transfer and internalization of FcRn into the interior of these organelles is a selective process.

Persistence of Rab5 on fusion-competent, late endosomes

Recent studies have shown that as early endosomes mature to form late endosomes, the Rab GTPase, Rab5, is gradually replaced by Rab7 (22). The observation that endosomal-lysosomal transfer events invariably involve FcRn$^+$ endosomes, from which FcRn can still recycle (Figure 3E, 3G, and data not shown), prompted us to characterize these compartments further. We therefore analyzed the Rab associations with endosomal compartments as they mature, with the overall aim of characterizing the endosomes that are 'competent' to transfer their contents to lysosomes.

Cotransfection of Rab5-fluorescent protein (FP) with FcRn-FP constructs demonstrated that Rab5, consistent with its known function in earlier studies (17,18), can be detected on FcRn$^+$ endosomes. We observed that Rab5$^+$ FcRn$^+$ compartments can transfer FcRn to lysosomes in tubule-mediated processes such as that shown in Figure 5A. The tubule extends, contacts, and fuses with the lysosome and separates from the late endosome over a period of 12 s, with detectable transfer of mRFP-FcRn occurring over a

period of 3 s (12–15 s) (Figure 5A; The intensity changes for mRFP fluorescence in the interacting compartments and the photobleaching analysis for mRFP are shown in Figures S2A and S2B, respectively). Significantly, transfer of FcRn to lysosomes occurred without detectable transfer of Rab5 (Figure 5A). To exclude the possibility that Rab5 overexpression might result in mistargeting to late endosomes, we analyzed Rab5 distribution in untransfected cells using anti-Rab5 and anti-LAMP-1/anti-EEA1 antibodies. We consistently observed that Rab5 is associated with LAMP-1^+ late endosomes but not LAMP-1^+ lysosomes within cells (Figure 5B; 58% (n = 88) of Rab5$^+$ compartments are LAMP-1^+), indicating that Rab5 is not solely restricted to association with early endosomes. These late endosomes can be distinguished from lysosomes by the lower levels of LAMP-1 (Figure 4, and data not shown). In these studies, 96% of 54 late endosomes analyzed with lower LAMP-1 levels are Rab5$^+$, whereas 95% of 57 lysosomes analyzed with brighter LAMP-1 are Rab5$^-$. We frequently observed the accumulation of Rab5 into domains or clusters on these compartments (Figure 5B). This is reminiscent of the accumulation of Rab GTPases into discrete domains that precede the formation of tubulovesicular transport containers on endosomes (47–49). As expected from earlier studies (17), the colocalization between Rab5 and EEA1 is also extensive (Figure 5B; 100% of 52 EEA1$^+$ endosomes analyzed are Rab5$^+$). Complete loss of Rab5 from (late) endosomes is, therefore, not a prerequisite for the transfer of FcRn from late endosomes to lysosomes.

We also investigated whether fusion-competent endosomes were Rab7$^+$, and also whether transfer of Rab7 to lysosomes could be detected. HMEC-1 cells were therefore cotransfected with GFP-Rab7 and mRFP-FcRn. Figure 5C shows that Rab7 is present on both late endosomes and lysosomes, consistent with earlier observations (19,20). Figure 5D shows the transfer of Rab7

Figure 3: Analyses of transfer of labeled IgG to lysosomes indicate distinct processes. HMEC-1 cells were cotransfected with FcRn-GFP (human) and human β_2m (A) or FcRn-GFP (mouse) and mouse β_2m (C, E, and G). Cells were pulsed with Alexa 555-labeled dextran for 2 hours, chased for 1 hour and incubated with 5 μg/ml Atto 647N-labeled IgG for 7 (A), 5 (C), or 4 (E and G) hours. Individual images in A, C, E, and G are presented with the time (in seconds) at which each image was acquired (first image is arbitrarily set to time 0). Images shown in A, C and E are individual frames of Movie S3, S4 and S5, respectively. Scale bars = 1 μm. A, a dextran$^+$ IgG$^+$ lysosome (white arrowhead) interacts with an endosome (red arrowhead, FcRn$^+$ IgG$^+$ limiting membrane) for an extended time period (27–94.50 s, when data collection was stopped). Detectable levels of IgG are transferred from the endosome to the lysosome via a tubule (43.5–46.5 s). Events of interest are indicated by white arrows. The boxed region marked at 39 s is subsequently presented as cropped, single color (IgG) images in the lower row, with red arrows indicating the same event. B, fluorescence intensity plots for Atto 647N (IgG) in the lysosome and the endosome for A, with time of initiation of transfer indicated. C, a FcRn$^+$ IgG$^+$ late endosome (red arrowhead) interacts with a dextran$^+$ IgG$^+$ lysosome (white arrowhead) for a prolonged period (58.5–517.50 s, when data collection was stopped) to transfer IgG without detectable tubular extension(s). D, fluorescence intensity plots for Atto 647N (IgG) in the lysosome and the endosome for C, with time of initiation of transfer indicated. E, a FcRn$^+$ IgG$^+$ tubule, indicated by white arrows, extends from a donor endosome (red arrowhead) towards a dextran$^+$ IgG$^+$ lysosome (white arrowhead), and contacts this lysosome for 25.5 s (12–37.5 s) before retracting. Detectable levels of IgG are transferred from this tubule to the lysosome (30–33 s). A second tubule, indicated by yellow arrows, extends from the donor endosome and interacts with another endosome (6–52.5 s) prior to retracting. The boxed region at 30 s is presented as cropped, single color (IgG) images in the lower row, with red arrows indicating IgG transfer from the donor endosome to the lysosome. F, fluorescence intensity plots for Atto 647N (IgG) in the lysosome and the endosome for E, with time of initiation of transfer indicated. G, later frames corresponding to E, showing that a FcRn$^+$ IgG$^+$ tubule (white arrows) extends (205.5 s) and leaves (234 s) the donor endosome after the same endosome has interacted with the lysosome (E).
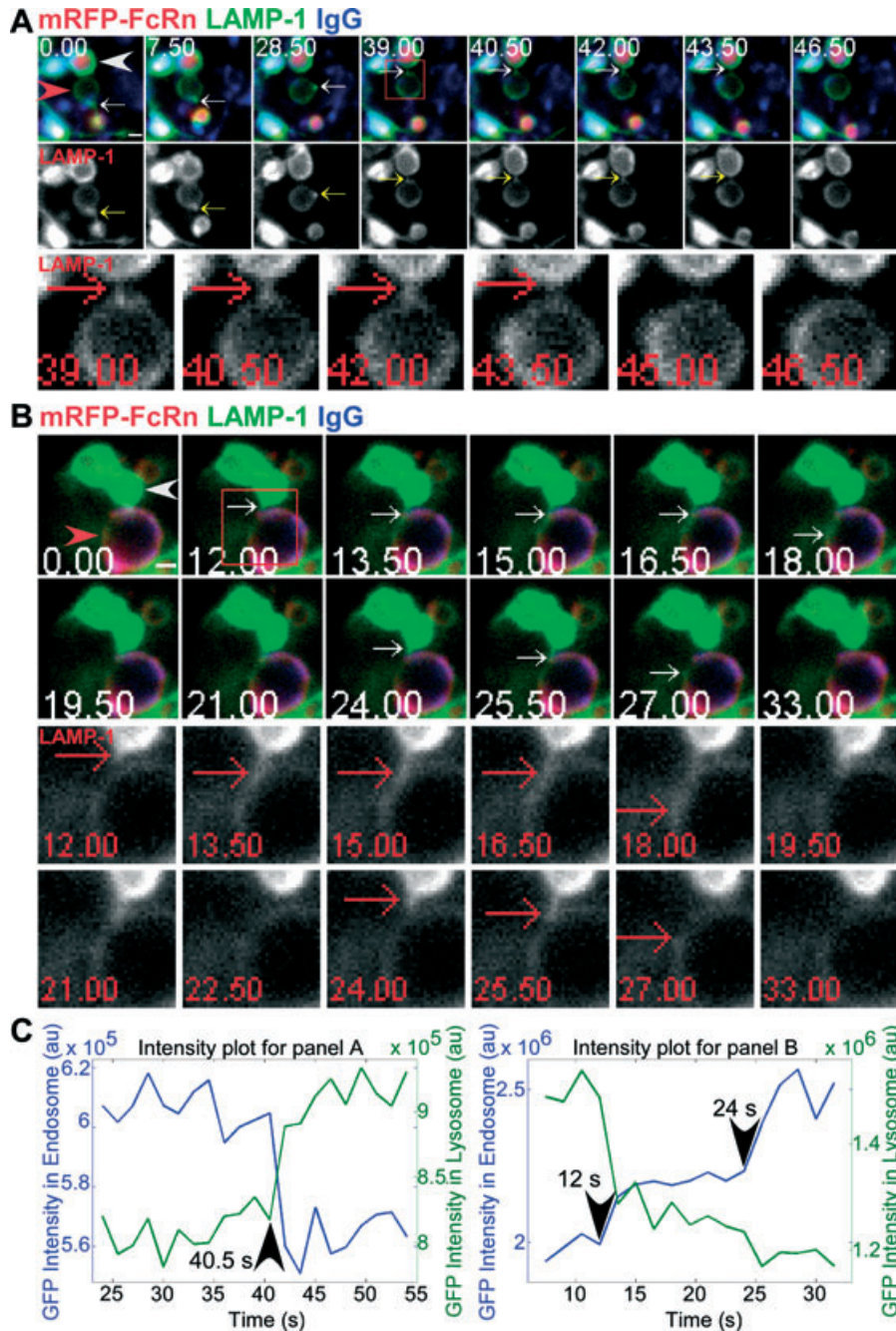
Figure 4: Bidirectional transfer of LAMP-1 involving tubules between late endosomes and lysosomes. HMEC-1 cells were cotransfected with LAMP-1-GFP, mRFP-FcRn (human), and human β_2m. Cells were incubated with Atto 647N-labeled IgG for 4.5 (A) or 3 (B) hours. Individual images in A and B are presented with the time (in seconds) at which each image was acquired (first image is arbitrarily set to time 0). Events of interest are indicated by white arrows. The boxed regions at 39 (A) or 12 (B) seconds are presented as cropped, single color (LAMP-1) images in the lower row(s), with red arrows indicating the same events. Images shown in A and B are individual frames of Movie S6 and S7, respectively. Scale bars = 1 μm. A, a tubule (white arrows) extending (0 s) from the lower part of a late endosome (red arrowhead), forms a vesicular compartment on the limiting membrane (7.5 s), moves around the perimeter of the late endosome, extends a tubule (39 s) and contacts (40.5 s) the limiting membrane of a lysosome (LAMP-1^+ limiting membrane; mRFP-FcRn$^+$ IgG$^+$ intraluminal space; white arrowhead), transfers LAMP-1 (40.5–43.5 s) and separates from the late endosome at 43.5 s. The LAMP-1 single color data is presented in the middle row, with the yellow arrows indicating the same tubulovesicular compartment. B, two different tubules extend sequentially (starting at 12 s) from a lysosome (white arrowhead) to a late endosome (red arrowhead) and transfer LAMP-1 over two time windows (12–18, 24–25.5 s), as indicated by white arrows. Subsequently, the LAMP-1 appears to diffuse into the limiting membrane of the late endosome. No transfer of mRFP-FcRn could be detected. C, the fluorescence intensity plots for LAMP-1-GFP in the interacting compartments in A and B, with times of initiation of transfer indicated.

to lysosomes. A Rab7$^+$ tubule extends from a late endosome at 27 s, contacts a FcRn-mRFP$^+$ dextran$^+$ lysosome at 39 s and transfers Rab7 over the following 3 s. The intensity changes for GFP fluorescence in the interacting compartments and the photobleaching analysis for GFP are shown in Figures S2C and S2D, respectively. Cotransfection of mRFP-Rab5 and GFP-Rab7 constructs

demonstrated that Rab5$^+$ Rab7$^+$ endosomes can interact with lysosomes over extended periods of time ($\sim$40 s) (Figure 5E). A small Rab5$^+$ compartment, that is most likely an endosome, is also associated with this lysosome. In all cases where endosomal-lysosomal interactions were observed (n = 22, from 11 different cells), Rab7 was detectable on the endosomal compartment (Figure 5D,

data not shown). Our data indicate that acquisition of Rab7, but not complete loss of Rab5, is necessary for late endosome-lysosome interactions. The accumulation of these Rab proteins into domains provides a mechanism whereby the late endosome can be compartmentalized into regions that have distinct intracellular fates.

Discussion

Despite the central role that lysosomes play in cellular homeostasis, how membrane receptors are delivered from the endocytic pathway for degradation remains an area of active investigation (2). In the current study, we have analyzed the intracellular trafficking processes that lead to the transfer of the Fc receptor, FcRn, from late endosomes to lysosomes. In contrast to previously described receptors (11), we demonstrate that FcRn does not enter ILVs in late endosomes prior to lysosomal delivery. The pathway that this receptor takes in transit to lysosomes is therefore distinct to the ubiquitin-dependent and -independent processes for ILV entry (7–11). In this context, the lysine residue in the cytosolic tail of human FcRn is not conserved in mouse FcRn (45,46), and the similar behavior of mouse and human FcRn therefore indicate that the trafficking of this receptor is ubiquitin-independent. Our analyses also demonstrate that FcRn delivery to lysosomes occurs via fusion processes that usually involve tubular transport or organellar interactions that resemble kiss-and-linger (5,6,35,36), rather than complete merging of the participating organelles.

Our data are consistent with the following model that encompasses several novel features for the lysosomal delivery of membrane receptors (Figure 6). The receptor is present on the membrane of $Rab5^+$ early endosomes that mature into $Rab5^+$ $Rab7^+$ late endosomes. Recycling/transcytotic receptors such as FcRn that remain on the limiting membrane can segregate from these endosomes into the recycling/transcytotic pathway, or enter lysosomes via processes that usually employ tubular connections or resemble kiss-and-linger events (5,6,35,36) but do not involve 'backflow' of lysosomal contents. This functional plasticity of endosomes is congruent with the formation of membrane domains that are characterized by distinct compositions of Rab GTPases and lipids (47,49,50). Transfer can be mediated by an extension of a tubule from one compartment to another, or by direct contact of the two compartments. By contrast, complete fusion of late endosomes and lysosomes is rarely observed. Transfer by tubular extensions would be expected to limit content mixing, and might be analogous to the exocytic processes that involve direct endosomal-plasma membrane connections that we have described previously (43). Interestingly, tubules can either retract back towards, or separate from, their donor organelle following or during transfer of material to lysosomes. Movement of the Fc receptor, FcRn, from the late endosome to the lysosome is rapidly followed by internalization

into the intraluminal space, via a process that might resemble ILV internalization in MVBs/late endosomes (11). By contrast, proteins such as LAMP-1 migrate in a bidirectional fashion between the limiting membranes of late endosomes and lysosomes. The model also incorporates features concerning the behavior of the Rab GTPases, Rab5 and Rab7. Although Rab7 acquisition appears to be a prerequisite for a late endosome to reach a state of fusion competence with lysosomes, complete loss of Rab5 is unexpectedly not.

The dominance of selective transfer processes such as via tubular connections, rather than complete fusion, during lysosomal delivery has several important consequences: first, it provides a mechanism for the exclusion of Rab5 transfer to lysosomes, which, if it occurred, could promote (early) endosomal-lysosomal fusion (17,18) with concomitant degradation of endosomal contents. Second, in a more general sense, tubular transfer and kiss-and-linger type modes allow late endosomes to retain functional plasticity so that receptors on the limiting membrane can be selectively recycled or degraded. By extending the window of time during which recycling can occur, this might improve the fidelity of this process. Third, these transfer modes remove the necessity for organelle retrieval from hybrid compartments (2,5).

We observe that FcRn transfer to lysosomes occurs without detectable 'backflow' of lysosomal contents such as dextran to late endosomes. The involvement of tubular extensions with large surface area to volume ratios could regulate this. In this context, size selective transfer of dextran between compartments on the endocytic, phagocytic and exocytic pathways has been shown to occur in several distinct cell types (51–54). Constriction of the tubule could also occur in the vicinity of the truncation point with the donor organelle for tubules that separate, or closer to their 'fusing' end for tubules that retract back to their donor organelle. Such processes might also, for example, play a role in limiting endosomal release in exocytic pathways where tubular connections undergo exocytosis whilst retaining endosomal connectivity (43).

A study that is complementary to our analyses has described the processes that are involved in the transfer of the lumenal content of late endosomes to lysosomes in rat kidney fibroblast cells (5). Full fusion events between late endosomes and lysosomes were observed relatively frequently, and transfer of dextran between organelles occurred during kiss-and-run/kiss-and-linger events. These differences in mechanisms for membrane receptor and luminal content transfer suggest that late endosomes might have specific stages of maturation that are active in the transfer of these distinct constituents. Consistent with this, others have shown that not all endosomes or late endosomes/MVBs in a given cell are functionally equivalent (22,55).
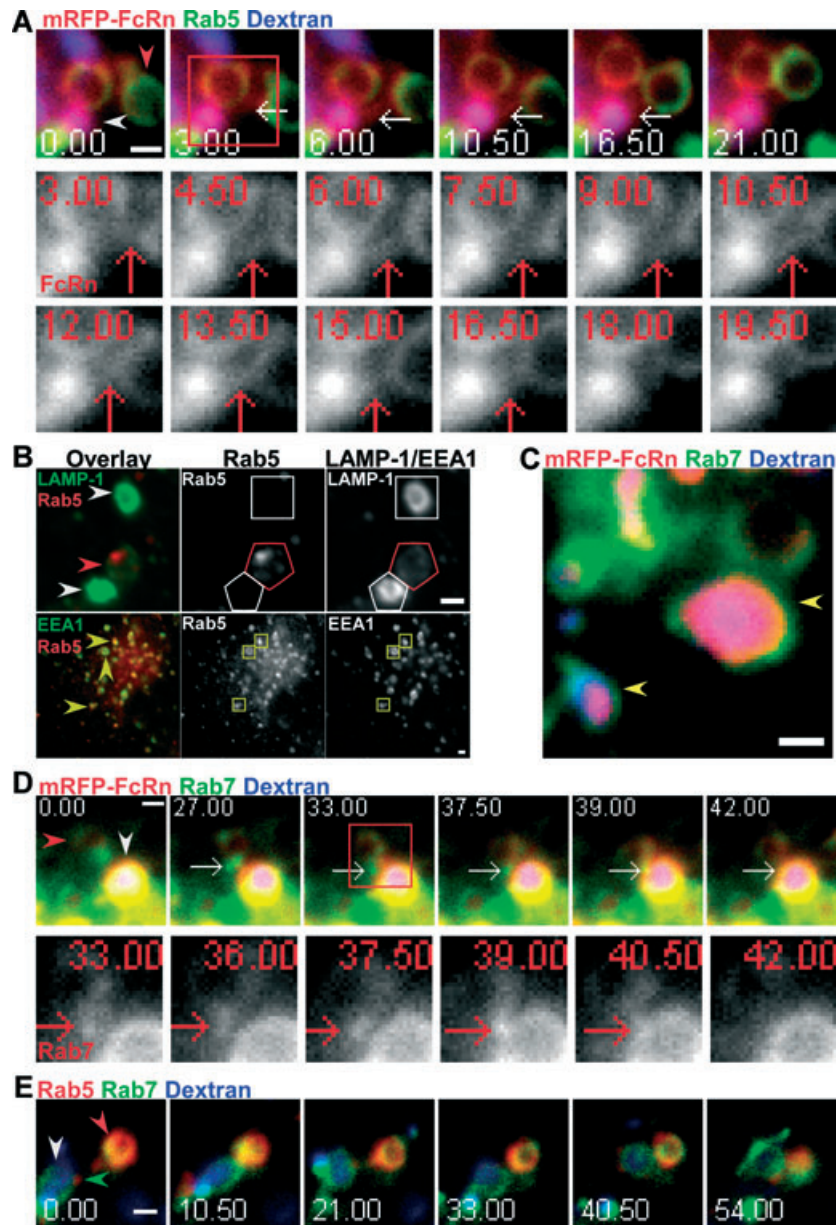
Figure 5: Legend on next page.

Following transfer from the limiting membrane of late endosomes, FcRn enters the intraluminal space of the lysosome. This contrasts with the behavior of the lysosomal membrane protein, LAMP-1, which migrates bidirectionally between the limiting membranes of late endosomes and lysosomes without detectable levels of FcRn. This suggests that the transfer and/or entry of FcRn into the lysosomal lumen is driven by a selective process that has not, to our knowledge, been described. Such a process could also be relevant for other, as yet unidentified, membrane receptors that do not enter ILVs in late endosomes (or MVBs) via ubiquitin-dependent or -independent processes (7–11). The question therefore arises as to why distinct lysosomal entry pathways exist

for different endocytic receptors. This could be related to a fundamental difference between the pathways taken on the constitutive versus stimulated degradative pathways; stimulated pathways necessitate the degradation of essentially all relevant receptor cargo whereas constitutive breakdown only applies to a fraction of the receptor load in late endosomes. In addition, ILV entry into MVBs is known to extinguish signaling of receptors such as EGFR (56), and a process that shortens the period of signaling activity post-internalization might be advantageous.

Recent studies have reported that early endosomal maturation to late endosomes is accompanied by gradual

Figure 5: Associations of the Rab GTPases, Rab5 and Rab7, with late endosomes that interact with lysosomes. HMEC-1 cells were cotransfected with GFP-Rab5, mRFP-FcRn (human) and human β_2m (A), GFP-Rab7, mRFP-FcRn (human) and human β_2m (C, D), or mRFP-Rab5 and GFP-Rab7 (E). Cells were pulsed with Alexa 647-labeled dextran for 2 hours and chased for 2 (A), 5 (C), 4 (D), or 6 (E) hours. Individual images in A, D and E are presented with the time (in seconds) at which each image was acquired (first image is arbitrarily set to time 0). Images shown in A and D are individual frames of Movie S8 and S9, respectively. Scale bars = 1 μm. A, a FcRn$^+$ Rab5$^-$ tubule, as indicated by white arrows, extends (3 s) from an endosome (mRFP-FcRn$^+$ Rab5$^+$ limiting membrane; red arrowhead), contacts a lysosome (mRFP-FcRn$^+$ dextran$^+$ intraluminal space; white arrowhead) between 4.5 and 6 s and transfers mRFP-FcRn over a period of 3 s (12–15 s). The boxed region at 3 s is subsequently presented as cropped, single color (mRFP-FcRn) images in the lower two rows. The intensity plots for mRFP-FcRn in the interacting compartments and the photobleaching analysis for mRFP-FcRn are shown in Figures S2A and S2B, respectively. B, HMEC-1 cells were fixed, permeabilized and stained with anti-EEA1 or LAMP-1 and anti-Rab5 antibodies. Compartments in the single color data for Rab5, EEA1 and LAMP-1 are highlighted with polygons of the same colors as the arrowheads. The red arrowhead in the upper left panel indicates a LAMP-1^+ Rab5$^+$ late endosome. The accumulation of Rab5 into discrete domains or clusters on the late endosome can be observed in the Rab5 single color and overlay data. White arrowheads in the upper left panel indicate lysosomes with higher LAMP-1 levels than the late endosome. There is no detectable Rab5 in the lysosomes. Yellow arrowheads in the lower left panel indicate Rab5$^+$ EEA1$^+$ compartments. C, yellow arrowheads indicate mRFP-FcRn$^+$ dextran$^+$ lysosomes with Rab7 on the limiting membrane. D, a Rab7$^+$ tubule, indicated by white arrows, extends (27 s) from a late endosome (mRFP-FcRn$^+$ Rab7$^+$ limiting membrane; red arrowhead), contacts (39 s) a lysosome (mRFP-FcRn$^+$ dextran$^+$ intraluminal space; white arrowhead) and transfers Rab7 over a 3 s period (39–42 s). The boxed region at 33 s is presented as cropped, single color (Rab7) images in the lower row. The intensity plots for GFP-Rab7 in the interacting compartments and the photobleaching analysis for GFP-Rab7 are shown in Figures S2C and S2D, respectively. E, a lysosome (Rab7$^+$ limiting membrane and dextran$^+$ intraluminal space; white arrowhead) interacts with a Rab5$^+$ Rab7$^+$ endosome (red arrowhead) from 10.50 s onwards. The green arrowhead indicates a small Rab5$^+$ endosome interacting with the lysosome.

replacement of Rab5 by Rab7 (22). Based on these analyses, a model in which all Rab5 is lost from late endosomes before they are competent to fuse with lysosomes has been proposed (22). Our data demonstrate that Rab5 can persist on the membrane of late endosomes during their interactions with lysosomes. In this context, others have shown that this Rab is involved in trafficking at late stages of the endolysosomal pathway (53,57). Further, although the lysosomes in HMEC-1 cells are Rab7$^+$, they lack Rab5, which is consistent with multiple earlier studies (17–20). In combination with the propensity of Rabs to form discrete domains on endosomes (47), this is congruent with the selective transfer of membrane (associated) proteins to lysosomes during late endosomal-lysosomal interactions.

Although not a central focus of the current study, our analyses bear some relevance to the intracellular fate of engineered IgGs, which in turn impacts *in vivo* behavior. The IgG that is used in this study is an engineered variant of human IgG1 that, relative to wild-type IgG1, binds to FcRn with enhanced affinity in the pH range 6.0–7.4 (41). IgGs of this class have short *in vivo* half-lives (58). In the current study, we show that this IgG, which remains tightly associated with FcRn and is not released during exocytic events (41,44), accumulates in lysosomes following several hours of uptake into FcRn$^+$ cells. This degradative fate provides a molecular explanation for the reduced whole body persistence. By contrast, wild-type IgGs that bind to FcRn at pH 6.0 but not detectably at near-neutral pH are salvaged from lysosomal degradation in FcRn expressing cells by recycling/transcytosis followed by exocytic release (23,44). Consequently, such IgGs have relatively long *in vivo* half-lives.

In summary, we have elucidated the pathways by which the Fc receptor, FcRn, undergoes constitutive degradation. These analyses reveal several novel aspects of endosomal/lysosomal trafficking and have led to a model that could be generally relevant to other membrane receptors. Our studies demonstrate that late endosomal contents are not irreversibly destined for lysosomal degradation, with the dominant mechanism of lysosomal delivery involving selective transfer by tubular extensions or kiss-and-linger-like processes. We also show that following transfer from the limiting membrane of late endosomes to lysosomes, FcRn accumulates in the intraluminal space of these compartments in a pathway that distinguishes it from other previously characterized receptors that enter ILVs in late endosomes/MVBs prior to lysosomal delivery. These studies are of relevance to understanding the processes that regulate the degradation of membrane receptors within cells.

Materials and Methods

Plasmid constructs

Plasmids encoding human and mouse FcRn tagged at the N- or C-terminus with enhanced GFP or mRFP, and human or mouse β_2-microglobulin (β_2m), have been described (23,41). A mutated variant of human FcRn ('79-89/136-147') that has higher affinity for binding to IgG (42) was used in human FcRn expression constructs. The nomenclature of the FcRn constructs used in this study is as follows: GFP-FcRn, FcRn with GFP appended to N-terminus; FcRn-GFP, FcRn with GFP appended to C-terminus etc.

An expression plasmid encoding LAMP-1-GFP (rat) was a generous gift of Prof. P. Luzio (University of Cambridge, UK). Plasmids to express Rab5 and Rab7 N-terminally tagged with enhanced GFP were generously provided by Prof. M. Zerial (Max Planck Institute of Molecular Cell Biology and Genetics, Germany). To generate plasmids to express mRFP-Rab5 and mRFP-Rab7, the Rab genes in GFP-Rab5 and GFP-Rab7 were recloned into a vector derived from pEGFP-C1 (Clontech) in which the enhanced
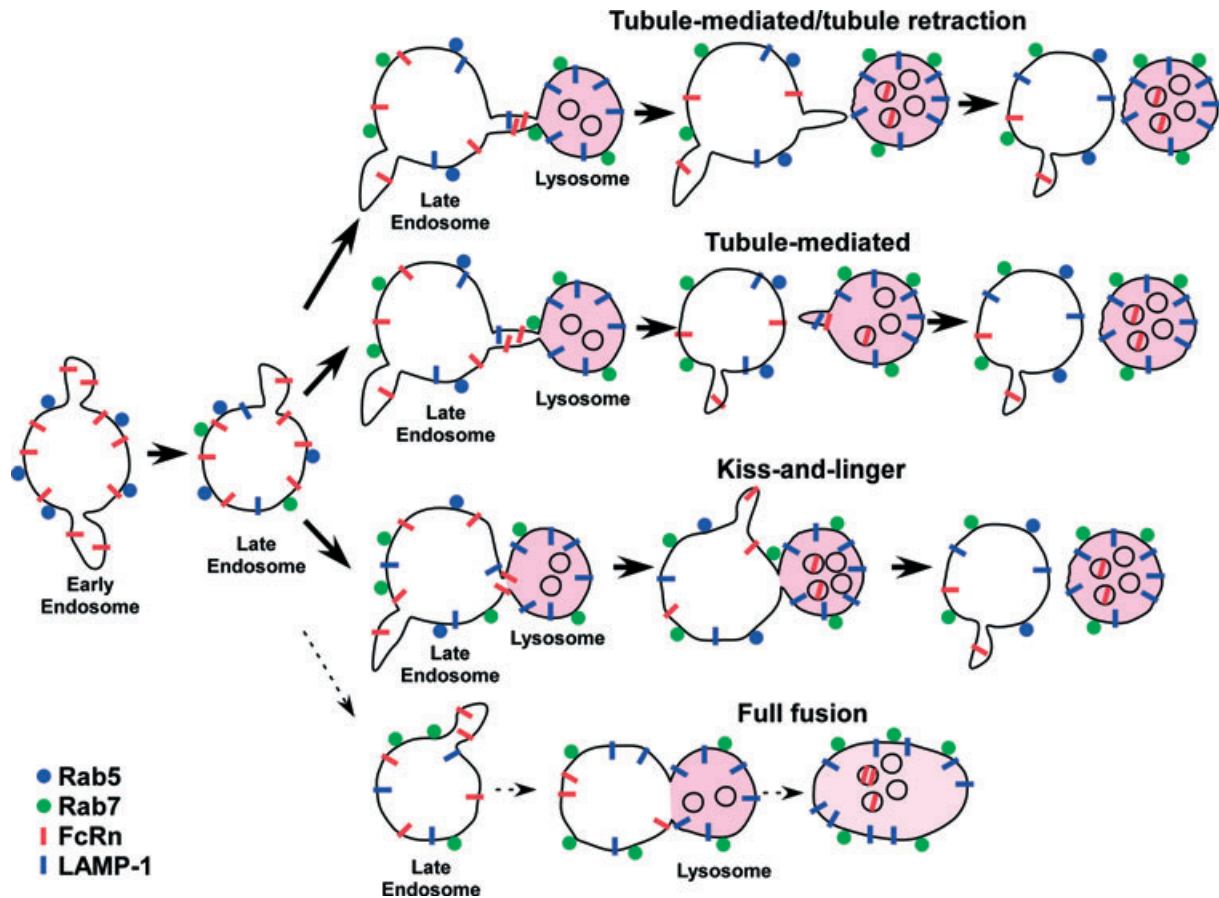
Figure 6: A model for the transfer of FcRn from late endosomes to lysosomes. Rab5$^+$ FcRn$^+$ early endosomes can mature to Rab5$^+$Rab7$^+$ late endosomes. The receptors remain on the limiting membrane of late endosomes and can either enter the recycling/transcytotic pathways or lysosomes. Transfer of FcRn from the limiting membrane of late endosomes to lysosomes can occur via several different processes as indicated. FcRn transfer to lysosomes is rapidly followed by internalization into the intraluminal space of lysosomes, whereas LAMP-1 persists on the limiting membrane. The lower frequency of full fusion events relative to the other types of processes is indicated by a dotted arrow.

GFP gene was replaced by the gene encoding mRFP (59) as an *Nhe*I-*Bgl*II fragment. The genes encoding Rab5 and Rab7 were recloned into the mRFP vector as *Kpn*I-*Bam*HI and *Bgl*II-*Eco*RI fragments, respectively.

Reagents and antibodies
Alexa 488, 555, and 647-labeled dextran (10,000 MW, anionic, fixable) were obtained from Invitrogen (Carlsbad, CA). A mutated version of human IgG (MST-HN) that has been engineered to bind through its Fc region with higher affinity to FcRn in the range pH 6.0–7.4 has been described (41). This IgG was labeled with Atto 647N-NHS ester (Atto-Tec, Siegen, Germany) as recommended by the manufacturer's methods.

Mouse IgG2a anti-Rab5 and mouse IgG1 anti-EEA1 antibodies were purchased from BD Biosciences (San Jose, CA). Mouse IgG1 anti-LAMP-1 antibody (H4A3) was purchased from the Developmental Studies Hybridoma Bank (Iowa City, IA). Alexa 488-labeled goat anti-mouse IgG2a and Alexa 555-labeled goat anti-mouse IgG1 antibodies were purchased from Invitrogen.

Sample preparation
The human endothelial cell line HMEC-1 was generously provided by F. Candal at the CDC (Atlanta, GA) and maintained as in Ref. (23). HMEC-1 cells were transiently cotransfected with different combinations of

expression constructs using Nucleofector technology (Amaxa Biosystems, Cologne, Germany) as described in Ref. (23). These combinations are: FcRn-GFP (human) (1 µg) and human β_2m (1 µg); FcRn-GFP (mouse) (1 µg) and mouse β_2m (1 µg); mRFP-FcRn (human) (1 µg) and human β_2m (1 µg); FcRn-mRFP (human) (1 µg) and human β_2m (1 µg); LAMP-1-GFP (rat) (1 µg), mRFP-FcRn (human) (1 µg), and human β_2m (1 µg); GFP-Rab5 (0.5 µg), mRFP-FcRn (human) (1 µg), and human β_2m (1 µg); GFP-Rab7 (0.5 µg), mRFP-FcRn (human) (1 µg), and human β_2m (1 µg); mRFP-Rab5 (0.5 µg) and GFP-Rab7 (0.5 µg).

For pulse-chase studies with labeled dextran, cells were incubated with Alexa 488, 555 or 647-labeled dextran (500 µg/ml in phenol red-free HAM's F-12 K medium at ≈ pH 7.4) for 2 hours. Cells were then washed and chased in phenol red-free HAM's F-12 K medium at ≈ pH 7.4 for 1–6 hours. For incubation with Atto 647N-labeled IgG (MST-HN mutant), cells were incubated with 5 µg/ml IgG in phenol red-free HAM's F-12 K medium at ≈ pH 7.4 for 1–24 hours.

For immunofluorescence studies, cells were fixed using 3.4% paraformaldehyde (15 min at room temperature) and permeabilized using 0.5 mg/ml saponin in phosphate buffered saline (PBS). Cells were then incubated with 1 µg/ml mouse IgG2a anti-Rab5 and mouse IgG1 anti-LAMP-1 or mouse IgG1 anti-EEA1 primary antibodies in 1% BSA in PBS.

Following a 25-min incubation at room temperature, cells were washed in PBS, and bound antibodies detected by incubation with 2 µg/ml Alexa 488-labeled goat anti-mouse IgG2a and Alexa 555-labeled goat anti-mouse IgG1 antibodies for 25 min at room temperature. Cells were washed and mounted in Prolong (Invitrogen).

Fluorescence microscopy

For Figures 1A, B and 5B, images were acquired using a Zeiss (Thornwood, NY) Axiovert 200 M inverted fluorescence microscope with a Zeiss 1.4 NA $100\times$ Plan-APOCHROMAT objective and a Zeiss $1.6\times$ Optovar. Exciter HQ 470/40x, dichroic Q495LP, and emitter HQ 525/50m were used for Alexa 488, exciter HQ 545/30x, dichroic 570LP, and emitter HQ 593/40m were used for mRFP or Alexa 555 and exciter HQ 640/20x, dichroic Q660LP, and emitter HQ 700/75m were used for Atto 647N or Alexa 647. All filters and dichroics were purchased from Chroma Technology (Brattleboro, VT). Images were acquired with a Hamamatsu Orca 100 CCD camera (Bridgewater, NJ).

For the lower panel of Figure 1A and all other images, cells were maintained at $35-37^\circ$C using an objective heater. Data were collected using a Zeiss Axiovert S100TV inverted fluorescence microscope with a Zeiss 1.4 NA $100\times$ Plan-APOCHROMAT objective and a Zeiss $1.6\times$ Optovar. A custom-built laser excitation system using a right side-facing filter cube has been described previously (23,44,49). Three laser lines were used for wide-field excitation. A 488-nm laser (Laser Physics, West Jordan, UT) was used for GFP excitation, a 543-nm laser (Research Electro-Optics, Boulder, CO) for mRFP or Alexa 555 excitation and, a 633-nm laser (JDS Uniphase, San Jose, CA) for Atto 647N or Alexa 647 excitation. Images were acquired with an Andor (South Windsor, CT) iXon camera. A beamsplitter 488/543/633 and emission filters Z488/543/633m, HQ590/50m, HQ525/50m, and HQ690/90m from Chroma Technology were used. The exposure time for each color was 500 ms, and a set of images for three colors was acquired every 1.5 s.

Image analysis

All data were processed and displayed using the custom-written Microscopy Image Analysis Tool (MIATool) software package (www4. utsouthwestern.edu/wardlab) in MATLAB (Mathworks, Natick, MA). The intensities of acquired data were linearly adjusted. Images were overlaid and annotated. In overlay images, the intensities of the individual color channels were adjusted to similar levels. When necessary, images were expanded to visualize the events of interest. This expansion resulted in pixelation. The final images were exported for presentation in Canvas 9 (ACD Systems, Miami, FL).

For intensity analyses of mRFP (FcRn; Figure 2C and Figure S2A), Atto 647N (IgG; Figure 3B, D and F) and GFP (LAMP-1; Figure 4C, Rab7; Figure S2C), regions of interest (ROIs) were segmented manually from the mRFP (FcRn), Atto 647N (IgG) or GFP (LAMP-1 or Rab7) channel images, respectively, and a threshold value was applied to the ROIs to determine pixels belonging to these compartments. A background intensity value was subtracted from each pixel in these compartments. The resulting values were added together to obtain the total mRFP (FcRn), Atto 647N (IgG) or GFP (LAMP-1 or Rab7) fluorescence intensities of the compartments. For photobleaching analyses, a background intensity value was subtracted from each pixel. The average intensities per pixel of the complete image for each frame were multiplied by the maximum pixel numbers of the donor compartments, and the resulting values were plotted over time.

Acknowledgments

Supporting Information

Additional Supporting Information may be found in the online version of this article:

Figure S1: mRFP, Atto 647N (IgG) or GFP photobleaching analyses for Figures 2A (panel A), 2B (panel B), 3A (panel C), 3C (panel D), 3E (panel E), 4A (panel F) and 4B (panel G). A background intensity value was subtracted from each pixel. The average intensities per pixel of the complete image for each frame were multiplied by the maximum pixel numbers of the donor compartments, and the resulting values were plotted over time. The mean mRFP (A and B), Atto 647N (C, D and E) or GFP (F and G) intensity decays ($\approx$ 40 000, 20 000, 6000, 70 000, 12 000, 12 000 and 4000 units, respectively) during the transfer events shown in Figures 2A, 2B, 3A, 3C, 3E, 4A and 4B are significantly less than the measured mRFP (Figures 2A, B), Atto 647N (Figures 3A, C and E) or GFP (Figures 4A, B) intensity decreases ($\approx$ 300 000, 100 000, 150 000, 700 000, 150 000, 50 000 and 500 000 units, respectively) of the donor compartments shown in Figures 2C, 3B, 3D, 3F and 4C. These photobleaching analyses indicate that the intensity decreases shown in Figures 2C, 3B, 3D, 3F and 4C are not only due to photobleaching. Our intensity plotting shows that in general the photobleaching profile of mRFP shows greater fluctuation than that of GFP and Atto 647N.

Figure S2: mRFP or GFP intensity analyses for Figures 5A and 5D. A, the fluorescence intensity plots for mRFP in the interacting compartments in Figure 5A, with time of initiation of transfer indicated. B, mRFP photobleaching analysis for Figure 5A. The mean mRFP decays ($\approx$ 0 unit) during the transfer events shown in Figure 5A is significantly less than the measured mRFP intensity decreases ($\approx$ 250 000 units) of the donor endosome shown in A, indicating that the intensity decreases shown in A are not due to photobleaching. C, the fluorescence intensity plots for GFP in the interacting compartments in Figure 5D, with time of initiation of transfer indicated. D, GFP photobleaching analysis for Figure 5D. The mean GFP decays ($\approx$ 50 000 units) during the transfer events shown in Figure 5D is significantly less than the measured GFP intensity decreases ($\approx$ 400 000 units) of the donor endosome shown in C, indicating that the intensity decreases shown in C are not only due to photobleaching.

Movie S1: Tubule-mediated transfer of FcRn from the limiting membrane of a late endosome to the intraluminal space of a lysosome. The movie corresponds to Figure 2A. mRFP-FcRn is shown in red, and LAMP-1 is shown in green in the overlay data. The right column shows the single color (mRFP-FcRn) data. Arrows indicate events of interest as described in the figure legend. Movie plays at nine times the acquisition speed. Scale bar = 1 µm.

Movie S2: Tubule-mediated transfer of FcRn from the limiting membrane of a late endosome to the intraluminal space of a lysosome. The movie corresponds to Figure 2B. mRFP-FcRn is shown in red, and LAMP-1 is shown in green in the overlay data. The right column shows the single color (mRFP-FcRn) data. Arrows indicate events of interest as described in the figure legend. Movie plays at six times the acquisition speed. Scale bar = 1 µm.

Movie S3: Tubule-mediated transfer of labeled IgG to a lysosome. The movie corresponds to Figure 3A. Dextran is shown in red, FcRn-GFP is shown in green, and IgG is shown in blue in the overlay data. The right column shows the single color (IgG) data. Arrows indicate events of interest as described in the figure legend. Movie plays at three times the acquisition speed. Scale bar = 1 µm.

Movie S4: IgG is transferred to a lysosome in an interaction that resembles kiss-and-linger. The movie corresponds to Figure 3C. Dextran is shown in red, FcRn-GFP is shown in green, and IgG is shown in blue

in the overlay data. Arrows indicate events of interest as described in the figure legend. Movie plays at nine times the acquisition speed. Scale bar = 1 μm.

Movie S5: Tubule-mediated transfer of labeled IgG to a lysosome. The movie corresponds to Figure 3E. Dextran is shown in red, FcRn-GFP is shown in green, and IgG is shown in blue in the overlay data. The right column shows the single color (IgG) data. Arrows indicate events of interest as described in the figure legend. Movie plays at fifteen times the acquisition speed. Scale bar = 1 μm.

Movie S6: Tubule-mediated transfer of LAMP-1 from a late endosome to a lysosome. The movie corresponds to Figure 4A. mRFP-FcRn is shown in red, LAMP-1 is shown in green, and IgG is shown in blue in the overlay data. Arrows indicate events of interest as described in the figure legend. Movie plays at nine times the acquisition speed. Scale bar = 1 μm.

Movie S7: Tubule-mediated transfers of LAMP-1 from a lysosome to a late endosome. The movie corresponds to Figure 4B. mRFP-FcRn is shown in red, LAMP-1 is shown in green, and IgG is shown in blue in the overlay data. The middle and right columns show the single color (LAMP-1 and mRFP-FcRn, respectively) data. Arrows indicate events of interest as described in the figure legend. Movie plays at three times the acquisition speed. Scale bar = 1 μm.

Movie S8: Transfer of FcRn to a lysosome from a Rab5$^+$ endosome. The movie corresponds to Figure 5A. mRFP-FcRn is shown in red, Rab5 is shown in green, and dextran is shown in blue in the overlay data. The right column shows the single color (mRFP-FcRn) data. Arrows indicate events of interest as described in the figure legend. Movie plays at nine times the acquisition speed. Scale bar = 1 μm.

Movie S9: Transfer of Rab7 from an endosome to a lysosome. The movie corresponds to Figure 5D. mRFP-FcRn is shown in red, Rab7 is shown in green, and dextran is shown in blue in the overlay data. The single color data of mRFP-FcRn (the second column), Rab7 (the third column), and dextran (the fourth column) are also shown. Arrows indicate events of interest as described in the figure legend. Movie plays at three times the acquisition speed. Scale bar = 1 μm.

Please note: Wiley-Blackwell are not responsible for the content or functionality of any supporting materials supplied by the authors. Any queries (other than missing material) should be directed to the corresponding author for the article.

References

1. Holtzman E. Lysosomes. New York: Plenum Press; 1989.
2. Luzio JP, Pryor PR, Bright NA. Lysosomes: fusion and function. Nat Rev Mol Cell Biol 2007;8:622–632.
3. Vida T, Gerhardt B. A cell-free assay allows reconstitution of Vps33p-dependent transport to the yeast vacuole/lysosome. J Cell Biol 1999;146:85–98.
4. Bright NA, Reaves BJ, Mullock BM, Luzio JP. Dense core lysosomes can fuse with late endosomes and are re-formed from the resultant hybrid organelles. J Cell Sci 1997;110:2027–2040.
5. Bright NA, Gratian MJ, Luzio JP. Endocytic delivery to lysosomes mediated by concurrent fusion and kissing events in living cells. Curr Biol 2005;15:360–365.
6. Storrie B, Desjardins M. The biogenesis of lysosomes: is it a kiss and run, continuous fusion and fission process? Bioessays 1996;18:895–903.
7. Katzmann DJ, Babst M, Emr SD. Ubiquitin-dependent sorting into the multivesicular body pathway requires the function of a conserved endosomal protein sorting complex, ESCRT-I. Cell 2001;106:145–155.
8. Urbanowski JL, Piper RC. Ubiquitin sorts proteins into the intralumenal degradative compartment of the late-endosome/vacuole. Traffic 2001;2:622–630.
9. Reggiori F, Pelham HR. Sorting of proteins into multivesicular bodies: ubiquitin-dependent and -independent targeting. EMBO J 2001;20:5176–5186.
10. McNatt MW, McKittrick I, West M, Odorizzi G. Direct binding to Rsp5 mediates ubiquitin-independent sorting of Sna3 via the multivesicular body pathway. Mol Biol Cell 2007;18:697–706.
11. Piper RC, Katzmann DJ. Biogenesis and function of multivesicular bodies. Annu Rev Cell Dev Biol 2007;23:519–547.
12. Williams RL, Urbe S. The emerging shape of the ESCRT machinery. Nat Rev Mol Cell Biol 2007;8:355–368.
13. Razi M, Futter CE. Distinct roles for Tsg101 and Hrs in multivesicular body formation and inward vesiculation. Mol Biol Cell 2006;17:3469–3483.
14. Zerial M, McBride H. Rab proteins as membrane organizers. Nat Rev Mol Cell Biol 2001;2:107–117.
15. Pfeffer S, Aivazian D. Targeting Rab GTPases to distinct membrane compartments. Nat Rev Mol Cell Biol 2004;5:886–896.
16. Grosshans BL, Ortiz D, Novick P. Rabs and their effectors: achieving specificity in membrane traffic. Proc Natl Acad Sci U S A 2006;103:11821–11827.
17. Simonsen A, Lippe R, Christoforidis S, Gaullier JM, Brech A, Callaghan J, Toh BH, Murphy C, Zerial M, Stenmark H. EEA1 links PI(3) K function to Rab5 regulation of endosome fusion. Nature 1998;394:494–498.
18. Christoforidis S, McBride HM, Burgoyne RD, Zerial M. The Rab5 effector EEA1 is a core component of endosome docking. Nature 1999;397:621–625.
19. Soldati T, Rancano C, Geissler H, Pfeffer SR. Rab7 and Rab9 are recruited onto late endosomes by biochemically distinguishable processes. J Biol Chem 1995;270:25541–25548.
20. Bucci C, Thomsen P, Nicoziani P, McCarthy J, van Deurs B. Rab7: a key to lysosome biogenesis. Mol Biol Cell 2000;11:467–480.
21. Progida C, Malerod L, Stuffers S, Brech A, Bucci C, Stenmark H. RILP is required for the proper morphology and function of late endosomes. J Cell Sci 2007;120:3729–3737.
22. Rink J, Ghigo E, Kalaidzidis Y, Zerial M. Rab conversion as a mechanism of progression from early to late endosomes. Cell 2005;122:735–749.
23. Ober RJ, Martinez C, Vaccaro C, Zhou J, Ward ES. Visualizing the site and dynamics of IgG salvage by the MHC class I-related receptor, FcRn. J Immunol 2004;172:2021–2029.
24. Ghetie V, Ward ES. Multiple roles for the major histocompatibility complex class I-related receptor FcRn. Annu Rev Immunol 2000;18:739–766.
25. Dautry-Varsat A, Ciechanover A, Lodish HF. pH and the recycling of transferrin during receptor-mediated endocytosis. Proc Natl Acad Sci U S A 1983;80:2258–2262.
26. Maxfield FR, McGraw TE. Endocytic recycling. Nat Rev Mol Cell Biol 2004;5:121–132.
27. Simister NE, Mostov KE. An Fc receptor structurally related to MHC class I antigens. Nature 1989;337:184–187.
28. Dickinson BL, Badizadegan K, Wu Z, Ahouse JC, Zhu X, Simister NE, Blumberg RS, Lencer WI. Bidirectional FcRn-dependent IgG transport in a polarized human intestinal epithelial cell line. J Clin Invest 1999;104:903–911.
29. Firan M, Bawdon R, Radu C, Ober RJ, Eaken D, Antohe F, Ghetie V, Ward ES. The MHC class I related receptor, FcRn, plays an essential role in the maternofetal transfer of gammaglobulin in humans. Int Immunol 2001;13:993–1002.

30. Claypool SM, Dickinson BL, Yoshida M, Lencer WI, Blumberg RS. Functional reconstitution of human FcRn in Madin-Darby canine kidney cells requires co-expressed human beta 2-microglobulin. J Biol Chem 2002;277:28038–28050.

31. McCarthy KM, Yoong Y, Simister NE. Bidirectional transcytosis of IgG by the rat neonatal Fc receptor expressed in a rat kidney cell line: a system to study protein transport across epithelia. J Cell Sci 2000;113:1277–1285.

32. Ghetie V, Hubbard JG, Kim JK, Tsen MF, Lee Y, Ward ES. Abnormally short serum half-lives of IgG in beta 2-microglobulin- deficient mice. Eur J Immunol 1996;26:690–696.

33. Junghans RP, Anderson CL. The protection receptor for IgG catabolism is the beta2-microglobulin-containing neonatal intestinal transport receptor. Proc Natl Acad Sci U S A 1996;93:5512–5516.

34. Israel EJ, Wilsker DF, Hayes KC, Schoenfeld D, Simister NE. Increased clearance of IgG in mice that lack beta 2-microglobulin: possible protective role of FcRn. Immunology 1996;89:573–578.

35. Gandhi SP, Stevens CF. Three modes of synaptic vesicular recycling revealed by single-vesicle imaging. Nature 2003;423:607–613.

36. Ryan TA. Kiss-and-run, fuse-pinch-and-linger, fuse-and-collapse: the life and times of a neurosecretory granule. Proc Natl Acad Sci U S A 2003;100:2171–2173.

37. Patterson GH, Knobel SM, Sharif WD, Kain SR, Piston DW. Use of the green fluorescent protein and its mutants in quantitative fluorescence microscopy. Biophys J 1997;73:2782–2790.

38. Katayama H, Yamamoto A, Mizushima N, Yoshimori T, Miyawaki A. GFP-like proteins stably accumulate in lysosomes. Cell Struct Funct 2008;33:1–12.

39. Delamarre L, Pack M, Chang H, Mellman I, Trombetta ES. Differential lysosomal proteolysis in antigen-presenting cells determines antigen fate. Science 2005;307:1630–1634.

40. Daniels GM, Amara SG. Regulated trafficking of the human dopamine transporter. Clathrin-mediated internalization and lysosomal degradation in response to phorbol esters. J Biol Chem 1999;274:35794–35801.

41. Vaccaro C, Zhou J, Ober RJ, Ward ES. Engineering the Fc region of immunoglobulin G to modulate in vivo antibody levels. Nat Biotechnol 2005;23:1283–1288.

42. Zhou J, Mateos F, Ober RJ, Ward ES. Conferring the binding properties of the mouse MHC class I-related receptor, FcRn, onto the human ortholog by sequential rounds of site-directed mutagenesis. J Mol Biol 2005;345:1071–1081.

43. Prabhat P, Gan Z, Chao J, Ram S, Vaccaro C, Gibbons S, Ober RJ, Ward ES. Elucidation of intracellular recycling pathways leading to exocytosis of the Fc receptor, FcRn, by using multifocal plane microscopy. Proc Natl Acad Sci U S A 2007;104:5889–5894.

44. Ober RJ, Martinez C, Lai X, Zhou J, Ward ES. Exocytosis of IgG as mediated by the receptor, FcRn: An analysis at the single-molecule level. Proc Natl Acad Sci U S A 2004;101:11076–11081.

45. Ahouse JJ, Hagerman CL, Mittal P, Gilbert DJ, Copeland NG, Jenkins NA, Simister NE. Mouse MHC class I-like Fc receptor encoded outside the MHC. J Immunol 1993;151:6076–6088.

46. Story CM, Mikulska JE, Simister NE. A major histocompatibility complex class I-like Fc receptor cloned from human placenta: possible role in transfer of immunoglobulin G from mother to fetus. J Exp Med 1994;180:2377–2381.

47. Sönnichsen B, de Renzis S, Nielsen E, Rietdorf J, Zerial M. Distinct membrane domains on endosomes in the recycling pathway visualized by multicolor imaging of Rab4, Rab5, and Rab11. J Cell Biol 2000;149:901–914.

48. de Renzis S, Sönnichsen B, Zerial M. Divalent Rab effectors regulate the sub-compartmental organization and sorting of early endosomes. Nat Cell Biol 2002;4:124–133.

49. Ward ES, Martinez C, Vaccaro C, Zhou J, Tang Q, Ober RJ. From sorting endosomes to exocytosis: association of Rab4 and Rab11 GTPases with the Fc receptor, FcRn, during recycling. Mol Biol Cell 2005;16:2028–2038.

50. Pfeffer S. Membrane domains in the secretory and endocytic pathways. Cell 2003;112:507–517.

51. Berthiaume EP, Medina C, Swanson JA. Molecular size-fractionation during endocytosis in macrophages. J Cell Biol 1995;129:989–998.

52. Wang YL, Goren MB. Differential and sequential delivery of fluorescent lysosomal probes into phagosomes in mouse peritoneal macrophages. J Cell Biol 1987;104:1749–1754.

53. Duclos S, Corsini R, Desjardins M. Remodeling of endosomes during lysosome biogenesis involves 'kiss and run' fusion events regulated by rab5. J Cell Sci 2003;116:907–918.

54. Jaiswal JK, Chakrabarti S, Andrews NW, Simon SM. Synaptotagmin VII restricts fusion pore expansion during lysosomal exocytosis. PLoS Biol 2004;2:E233.

55. White IJ, Bailey LM, Aghakhani MR, Moss SE, Futter CE. EGF stimulates annexin 1-dependent inward vesiculation in a multivesicular endosome subpopulation. EMBO J 2006;25:1–12.

56. Katzmann DJ, Odorizzi G, Emr SD. Receptor downregulation and multivesicular-body sorting. Nat Rev Mol Cell Biol 2002;3:893–905.

57. Hirota Y, Kuronita T, Fujita H, Tanaka Y. A role for Rab5 activity in the biogenesis of endosomal and lysosomal compartments. Biochem Biophys Res Commun 2007;364:40–47.

58. Dall'Acqua W, Woods RM, Ward ES, Palaszynski SR, Patel NK, Brewah YA, Wu H, Kiener PA, Langermann S. Increasing the affinity of a human IgG1 to the neonatal Fc receptor: biological consequences. J Immunol 2002;169:5171–5180.

59. Campbell RE, Tour O, Palmer AE, Steinbach PA, Baird GS, Zacharias DA, Tsien RY. A monomeric red fluorescent protein. Proc Natl Acad Sci U S A 2002;99:7877–7882.